Open Medscience

Peer-Reviewed Open Access

JOURNAL OF DIAGNOSTIC IMAGING IN THERAPY

Journal homepage: www.openmedscience.com

Research Article

Quantitative *in vivo* Imaging of Adenosine A_{2A} Receptors in the Human Brain Using ^{11}C-SCH442416 PET: A Pilot Study

Igor D. Grachev [1,*], Miroslava Doder [2,†], David J. Brooks [2,3], Rainer Hinz[4]

[1] *Schering-Plough Research Institute, Kenilworth, NJ, USA*

[2] *MRC Clinical Sciences Centre and Division of Neuroscience, Faculty of Medicine, Imperial College, London, UK*

[3] *Hammersmith Imanet Ltd., GE Healthcare, Hammersmith Hospital, London, UK*

[4] *Wolfson Molecular Imaging Centre, University of Manchester, UK*

[†] *deceased*

[*] Author to whom correspondence should be addressed
Igor Grachev, M.D., Ph.D.
Independent R&D Pharmaceutical Consultant
T: +1 732 642 7773
grachevi@hotmail.com

Abstract:

^{11}C-SCH442416 was reported in preclinical studies with rodents and primates to be the first nonxanthine radioligand suitable for the *in vivo* imaging of adenosine A_{2A} receptors with positron emission tomography (PET). The aim of the present work was to investigate the suitability of ^{11}C-SCH442416 for the *in vivo* quantification of A_{2A} receptors in human brain.

Methods: Five male healthy subjects were scanned with 364 MBq bolus injections of ^{11}C-SCH442416. 90 minutes of dynamic PET emission data were acquired, and arterial blood samples

were taken throughout the scan to generate an arterial plasma input function. Using the individual MR images, regions-of-interest (ROIs) were defined for cerebellum, caudate, putamen and thalamus. Spectral analysis was used to determine the frequency components of the ^{11}C-SCH442416 tissue response for regional and voxel time-activity curves (TACs).

Results: ^{11}C-SCH442416 was rapidly metabolised in blood, the fraction of unmetabolised parent tracer in plasma being 41% at 15 minutes and 15% at 95 minutes, lower than that reported in rats and *macaca nemestrina*. No lipophilic radiolabelled metabolites were found in human plasma.

Rapid uptake of ^{11}C-SCH442416 was observed in all brain regions, reaching a maximum at about 3 minutes. When spectral analysis was applied to regional brain time activity curves (TACs), relatively rapid reversible region dependent and slower irreversible, region independent but subject specific components were identified. These components were further separated into irreversible nonspecific binding, reversible nonspecific binding, reversible specific binding and a blood component. Binding potentials of the nondisplaceable binding BP_{ND} were calculated using cerebellar volume of distribution as an estimate of the reversible nondisplaceable binding across the entire brain. Mean binding potentials BP_{ND} were: 2.5 (putamen), 1.6 (caudate) and 0.5 (thalamus).

Conclusion: Our study demonstrates that A_{2A} receptor binding can be quantified in striatal regions of the human brain with ^{11}C-SCH442416 PET. Despite the complex tracer kinetics and its low specific binding, reliable binding potentials could be estimated with spectral analysis.

Keywords: ^{11}C-SCH442416; adenosine A_{2A} receptor; PET; spectral analysis

1. Introduction

Adenosine is an endogenous modulator of neurotransmission that acts via an interaction with G-protein-coupled receptors in the central nervous system (CNS). Three major adenosine receptor subtypes have been identified: A_1, A_2 and A_3, with the adenosine A_2 receptors being subdivided into two further subtypes: A_{2A} and A_{2B} receptors. Adenosine A_{2A} receptors are abundant in the caudate-putamen, nucleus accumbens, and olfactory tubercle [1,2]. Although the roles of adenosine are not fully understood, it has been suggested that adenosine A_{2A} receptor activation may be involved in mediating a number of physiological functions in the CNS, including locomotion via regulation of the indirect striatal pathway to the internal pallidum and mood via its action on the ventral striatum. Potential therapeutic areas for agents acting at central A_{2A} receptors include schizophrenia, attention deficit hyperactivity disorder, anxiety disorders, depression, Huntington's disease, Gilles de la Tourette syndrome and Parkinson's disease.

For *in vivo* imaging studies using positron emission tomography (PET), several xanthine derivatives with A_{2A} receptor antagonist activity have been radiolabelled with the positron emitter carbon-11 (^{11}C).

^{11}C-KF1783 [3,4], ^{11}C-KF18446, ^{11}C-KF19631, ^{11}C-CSC [5], ^{11}C-KW-6002 [6,7] and ^{11}C-TMSX [8-10] have all been examined as markers of central A_{2A} receptors in preclinical models and humans.

^{11}C-KW-6002 showed potential as a PET ligand for quantifying striatal adenosine A_{2A} receptor function. However, cold KW-6002 partially blocked cerebellar binding of the tracer suggesting it was not a selective A_{2A} antagonist as this structure is reported to have low adenosine A_{2A} receptor density [7]. The A_1 selective antagonist KF15372 and the non-xanthine-type A_{2A} antagonist ZM 241385 both failed to block binding of ^{11}C-KW-6002 suggesting its cerebellar binding represented some other receptor class.

^{11}C-TMSX binding to A_{2A} receptors in the human brain has been reported [9,10]. Binding potentials were low, ranging from 1.25 in the anterior putamen followed by the caudate (1.05) and thalamus (1.03) down to 0.46 in the frontal lobe [10].

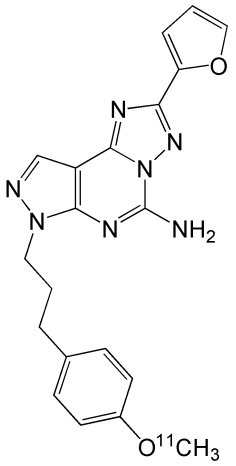

Figure 1. Chemical structure of ^{11}C-SCH442416.

In spite of numerous efforts to use labelled xanthine derivatives in PET imaging, their suitability as imaging biomarkers is limited by high nonspecific binding, relatively low signal-to-noise ratios and photoisomerization. Preclinical studies in rodents and primates suggest that ^{11}C-SCH442416 is a nonxanthine radioligand suitable for the *in vivo* imaging of adenosine A_{2A} receptors using positron emission tomography (PET) because of its high affinity and selectivity for adenosine A_{2A} receptors, good signal-to-noise ratio, and low levels of radioactive metabolite in the brains of nonhuman primates [11-14].

Here we present the results from the ^{11}C-SCH442416 PET study to demonstrate the feasibility of *in vivo* quantification of A_{2A} receptors with this imaging agent.

ISSN: 2057-3782 (Online)

http://dx.doi.org/10.17229/jdit.2014-0620-001

2. Materials and Methods

2.1. Subjects

Five male healthy subjects between the ages of 25 and 50 years (50, 30, 31, 25 and 26 years old; mean=32.4±10.2 years), body weight between 62.8 kg and 103.3 kg (mean = 78.2±16.27 kg), and Body Mass Index ranging from 19.2 to 28.9 kg/m^2 (mean = 23.88±4.11 kg/m^2) were enrolled into and completed this study.

Inclusion and exclusion criteria were chosen to ensure that a well-defined healthy subject population was included in the study. This included detailed medical history and complete physical examination, laboratory test results within normal range, normal vital signs, and normal or clinically acceptable 12-lead electrocardiogram (ECG). Exclusion criteria included any history or presence of clinically significant local or systemic infectious disease within 4 weeks prior to study drug administration, any significant medical disorder which would have required a physician's care, any history of seizures or autoimmune disorders, any history of mental instability; blood donation within 3 months before administration; history or presence of drug abuse; smoking more than 10 cigarettes or equivalent /day; subjects who have received radiation exposure (including x-rays) within 12 calendar months prior to the study; subjects with significant anatomical abnormalities noted on the MRI of the brain or any condition which would preclude MRI examination (e.g., implanted metal, severe claustrophobia); individuals who had evidence of only one patent arterial supply to the hand (Allen Test). All subjects had an indwelling venous cannula inserted into the median cubital vein of the forearm to inject the radioligand and also had an indwelling arterial cannula in the radial artery for the withdrawal of the blood samples.

This study was conducted in accordance with the Declaration of Helsinki Principles, ICH guidelines for Good Clinical Practice and after approval was obtained from the Research Ethics Committees at Central Middlesex and Hammersmith Hospitals, London; and the U.K. Administration of Radioactive Substances Advisory Committee (ARSAC). All subjects signed and dated an IEC-approved consent form before being enrolled into the study. All subjects were covered by Health Insurance System and/or in compliance with the recommendations of National Law in force relating to biomedical research.

2.2. PET/MRI scans

The radiotracer ^{11}C-SCH442416 was synthesized as previously described [11]. 364 MBq ± 11 MBq of ^{11}C-SCH442416 was injected by hand into an antecubital vein as a smooth bolus over 30 seconds (average injected volume was 1.9 mL ± 0.8 mL). Data for one subject could not be used because of an acquisition failure during the PET scan; thus data for four subjects were used in this study. The radiochemical purity was greater than 99% in all scans. The mass of co-injected cold SCH442416 was 2.13 µg ± 0.50 µg which is equivalent to a specific activity of 70.2 MBq/nmol ± 19.5 MBq/nmol.

All PET scans were performed on the high-sensitivity Siemens/CTI scanner ECAT EXACT3D with an axial field of view of 23.4 cm and 95 reconstructed transaxial image planes [15]. To reduce the effect of activity outside the direct field of view in brain scans, the tomograph was equipped with annular side shielding [16]. A 5-minute transmission scan using a ^{137}Cs point source was carried out prior to each study for subsequent attenuation and scatter correction [17]. The 90-minute 3D dynamic emission scan was acquired in list mode. In the post acquisition frame rebinning, 28 time frames of increasing length were generated (30s background frame prior to the injection, then 1 15s-frame, 1 5s-frame, 4 10s-frames, 4 60s-frames and 17 300s-frames). The spatial resolution of the images reconstructed using filtered back projection algorithm with the ramp and Colsher filters set to Nyquist frequency with the following set of parameters: scatter correction was model based; attenuation correction was measured and segmented; reconstruction machine was SUN CPU with a zoom 2.5; spatial resolution of reconstructed images was 5.1 mm x 5.1 mm x 5.9 mm (full width at half maximum [FWHM]); and reconstructed voxel size was 2.10 mm x 2.10 mm x 2.43 mm.

Arterial whole blood activity was monitored continuously for the first 15 minutes of the scan with a bismuth germanate coincidence detector [18] and the blood flow rate set to 5 mL/min for a fine temporal sampling of the radioactivity peak in the blood following the bolus injection. As this was the first-in-man study with ^{11}C-SCH442415, ten discrete arterial blood samples were initially taken at 5, 10, 15, 20, 30, 40, 50, 60, 75 and 95 minutes into heparinised syringes from which the activity concentration of the whole blood and that of the plasma were measured in a NaI well counter. This blood sampling protocol was a first guess based on the published data obtained in rats [11]. As it will be seen in the Results section, it was observed in the first two scans that the *in vivo* metabolism of ^{11}C-SCH442415 in humans was actually faster than reported in animals, therefore from the third scan on the blood sampling protocol was adapted such that the ten discrete arterial blood samples were subsequently taken at 3, 7, 11, 15, 20, 30, 45, 60, 75 and 95 minutes.

For the analysis of the radiolabelled compounds in plasma, all discrete blood samples except the 20 min sample (for subjects 1 and 2) or the 60 min sample (for subjects 3 and 4) were centrifuged at 11,000 rpm for 2 min to separate the plasma from the sample. Then the plasma sample was filtered using a 0.2 µm diameter filter, and an aliquot of the filtered sample of 1 mL was analyzed using solid-phase extraction with on-line reverse-phase HPLC radioactivity and UV detection [19]. The µ-Bondapak C_{18} column (300 mm x 7.8 mm internal diameter, 10 µm particle size) was washed with the mobile phase, a mixture of ammonium formate (0.1 M) and acetonitrile (35:65, v/v) at a flow rate of 3 mL/min. The eluate was monitored for radioactivity and UV absorbance at 310 nm. Both detectors were linked to a PC based integrator which recorded the chromatogram and enabled the correction for ^{11}C radioactivity decay and background and the integration of radioactive components. The amount of ^{11}C-SCH442416 and of the other radioactive components at each sample time was calculated as a percentage of each radioactive component in each analyte.

ISSN: 2057-3782 (Online)
http://dx.doi.org/10.17229/jdit.2014-0620-001

2.3. Definition of regions-of-interest (ROIs)

For each subject, brain magnetic resonance images (MRI) were acquired with T_1 weighted RF spoiled gradient echo volume scans on a 1 Tesla Philips Medical Systems HPQ+ Scanner. The echo time T_E was 6 ms, the repetition time T_R was 21 ms, the flip angle was 35˚, yielding an image resolution of 1.6 mm x 1.6 mm x 1.0 mm (AP, LR, HF respectively).

The individual MR images were coregistered to the PET images summed from 1 to 30 min after tracer injection using an automated multiresolution optimization procedure [20]. Six ROIs were defined manually on the individual MR image: left and right putamen, left and right caudate and left and right thalamus. The cerebellum was defined using a probabilistic brain atlas template [21,22]. Regional tissue time-activity curves were then generated from the dynamic images using the medical imaging software Analyze [23,24].

2.4. Data analysis

For the generation of the plasma input functions, the time course of the plasma-over-blood (POB) ratio, obtained from the first discrete arterial samples up to 20 min scan time, was fitted to an exponential approach to a constant value

$$POB\,(t) = p_1 \cdot \exp(-p_2 \cdot t) + p_3$$

with the three model parameters $p_1 > 0$, $p_2 > 0$ and $p_3 > 0$. For $t = 0$, the model function gives a POB value from the extrapolation of the measured data to zero.

$$POB\,(t{=}0) = p_1 + p_3 \ .$$

The measurement of the arterial whole blood activity obtained from the continuous detector system [18] was then multiplied with that POB ratio to obtain a total plasma activity curve for the first 15 min of the scan. This curve was then combined with the discrete plasma activity concentration measurements at 20, 30, 40 (subjects 1 and 2 only), 45 (subjects 3 and 4 only), 50 (subjects 1 and 2 only), 60, 75 and 95 minutes to generate an input function describing the total plasma activity concentration for the entire scan.

The input function of the activity concentration due to unmetabolised ^{11}C-SCH442416 in plasma was then created by multiplying the total plasma activity input function with the function obtained from the fit of the model for the parent fraction in plasma to the nine measurements of the parent compound during the scan. For the description of the parent fraction (PF) in plasma during the entire scan an exponential approach to a constant value was used as the mathematical model

$$PF\,(t) = (1 - q_2) \cdot \exp(- q_1 \cdot t) + q_2$$

with the two model parameters $q_1 > 0$ and $q_2 > 0$. Therefore, the initial value was always constrained to one

$$PF\,(t{=}0) = 1 \ .$$

Finally, the temporal delay of the arrival of the radioactivity bolus at the peripheral sampling site relative to the brain was determined [25].

Parameter estimates were obtained from fits of the measured tissue time-activity curves (no decay correction applied) minimizing the weighted sum of squares of the differences between the data and the model. The weights *w* for the individual data points were defined proportional to the reciprocal of the variance which was estimated from the scanner's rate of true coincidences *T* as

$$w_i = \frac{L_i}{T_i} \qquad \text{(for frame } i = 1, 2, 3, \ldots\text{)}$$

with *L* as the length of the frame [26].

Spectral analysis [27] of the regional tissue time-activity curves was performed with non-decay corrected data, using a library of 800 basis functions logarithmically spaced between the time constant of the radioactive decay of ^{11}C (λ= 5.663 x 10^{-4} s) and 10 s^{-1}.

The binding potential of the nondisplaceable binding BP_{ND} [28] was then calculated indirectly from the regional estimates of the total volume of distribution V_T

$$BP_{ND} = V_T^{\text{target region}} / V_T^{\text{cerebellum}} - 1,$$

using V_T of the cerebellum as an estimate of the free and nonspecifc binding of ^{11}C-SCH442416 throughout the brain. Cerebellum was previously reported from human autoradiographic studies as a region with a negligible density of A_{2A} receptors.

Spectral analysis [27] was also performed at a voxel level with the nonnegative least squares algorithm [29] as published in the Netlib (http://www.netlib.org/lawson-hanson) using 100 basis functions for the computational cost which were logarithmically spaced between the time constant of the radioactive decay of ^{11}C β_{min} = 5.663·x 10^{-4} s^{-1} ($\log_{10}$ β_{min} = -3.247) and β_{max} = 1 s^{-1} ($\log_{10}$ β_{max} = 0). For each peak in the spectrum (peak position β_i, peak height α_i), the contribution to the volume of distribution was obtained as $V_i = \frac{\alpha_i}{\beta_i - \lambda}$. From the set of *n* peaks the total volume of distribution V_T was calculated as $V_T = \sum_{i=1}^{n} V_i$ (excluding the peak representing the fractional blood volume).

All calculations were performed using Matlab® (The MathWorks, Inc., Natick, MA, USA) on Sun Ultra™ 10 workstations (Sun Microsystems, Inc., Santa Clara, CA, USA).

3. Results and Discussion

3.1. Input function

As reported from previous animal studies [11,13], blood ^{11}C-SCH442416 was initially distributed only in the plasma. A shows the time courses of the ratio of the plasma activity concentration over the whole blood activity concentration for all four subjects. With *H* as the haematocrit measured in the baseline blood sample before injection of the radioligand, the plasma-over-blood ratio extrapolated to

time zero by calculating $p_1 + p_3$ from the estimated parameters of the *POB* (*t*) model function agreed with the ratio $\frac{1}{1-H}$. Over the first 30 minutes of the scan, the plasma-over-blood activity ratio decreased. At later times the plasma-over-blood activity ratio rose again, consistent with the appearance of polar radiolabelled metabolites in the blood plasma.

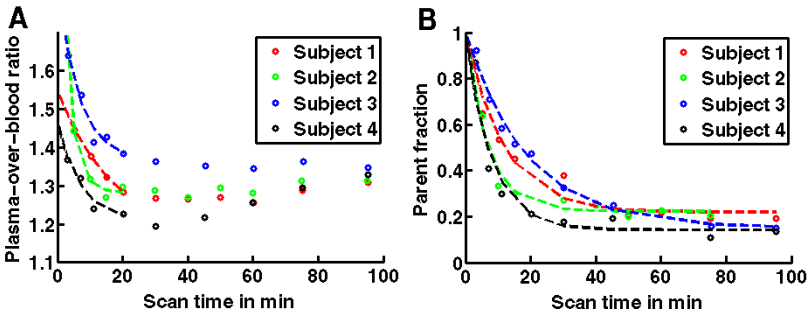

Figure 2. Time courses of the ratio of the plasma activity concentration over the whole blood activity concentration (A) and of the fraction of parent ^{11}C-SCH442416 in plasma (B) for the four subjects. The circles mark the measured data points, the dashed lines represent the fitted curves. Note the change of the sampling protocol from 5, 10, 15, 20, 30, 40, 50, 60, 75 and 95 minutes in subjects 1 and 2 to 3, 7, 11, 15, 20, 30, 45, 60, 75 and 95 min in subjects 3 and 4 to account for the faster metabolism of ^{11}C-SCH442415 in humans than reported in animals.

The radiochromatograms of the plasma radioactivity showed a minor polar radioactive component (retention time about 4.2 min) and a main component (retention time of 7.5 min) which was identified as ^{11}C-SCH442416 as it co-eluted with the same retention time as the unlabelled authentic standard of SCH442416. The other radioactive compounds observed in plasma were more polar than ^{11}C-SCH442416 but were not identified. The percentage of radioactive metabolites was observed to increase with time (B). The fraction of unmetabolized parent tracer in blood plasma averaged over the four subjects decreased from 87% at 3 minutes to about 41% at 15 minutes and 15% at 95 minutes post-injection, respectively. Therefore, the peripheral metabolism of ^{11}C-SCH442416 is faster in humans than previously reported in rats [11] and in a *macaca nemestrina* [13].

3.2. Tissue activity

There was rapid uptake of ^{11}C-SCH442416 in all brain regions. Inspection of the integral PET image from 1 to 30 minutes after injection reveals that the A_{2A} receptor rich striatal regions show higher activity than cortical brain areas and the cerebellum.

ISSN: 2057-3782 (Online)
http://dx.doi.org/10.17229/jdit.2014-0620-001

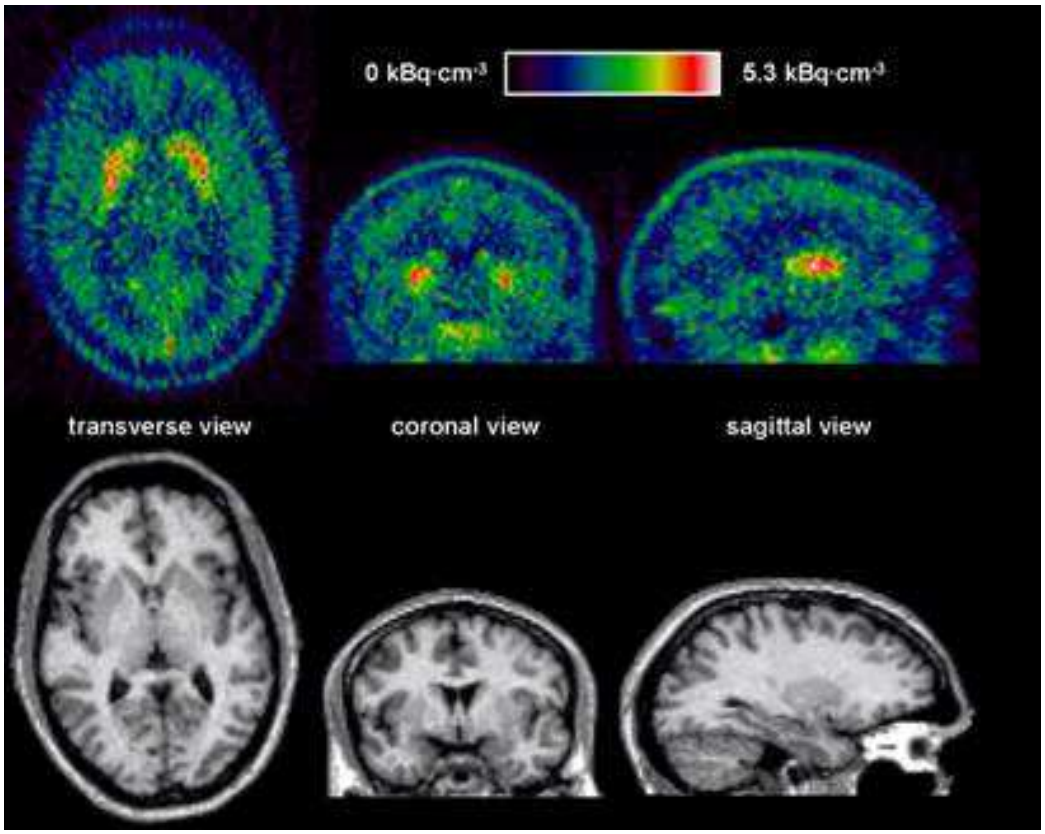

Figure 3. In the top row, a PET image summed from 1 to 30 min after bolus injection is shown. The T_1 weighted MR image in the bottom row is coregistered to the PET image. The highest activity concentrations are found in the A_{2A} receptor-rich striatum.

This shows that in all four subjects the tissue response functions reached a maximum on average at 3 minutes post bolus injection of the tracer. A relatively rapid reversible component of uptake was combined with a slower and apparently irreversible component with considerable inter-subject variability. In Subjects 1 and 3 (left) the rising plateau of irreversibly bound activity was much more marked than in Subjects 2 and 4 (right) whose tissue TACs showed mainly reversible characteristics reaching a nearly constant activity concentration at the end of the scans for all considered ROIs. The between subject variability in this cohort of four subjects is quite pronounced which complicates production of a coherent model describing the observed kinetics across regions and subjects.

ISSN: 2057-3782 (Online)
http://dx.doi.org/10.17229/jdit.2014-0620-001

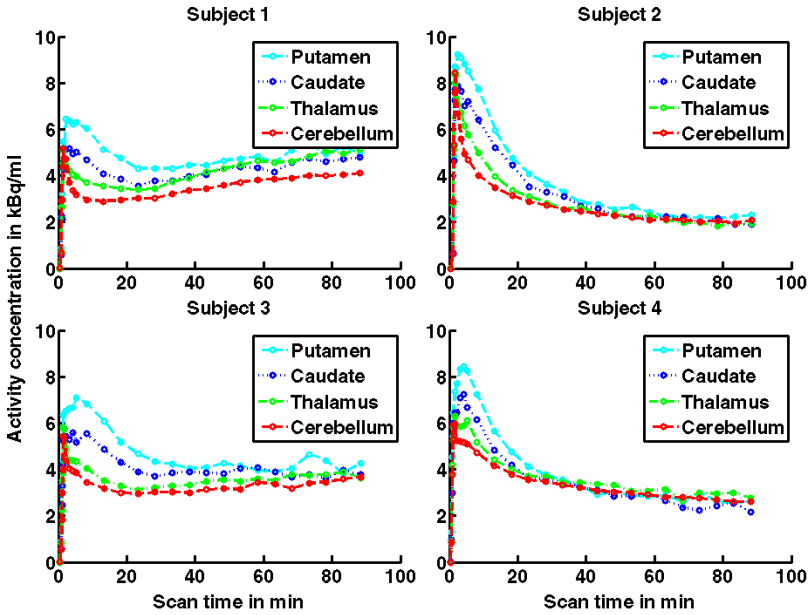

Figure 4. Tissue time-activity curves of the four scanned subjects, presented as decay-corrected data. The left and right regions are shown combined.

3.3. Kinetic analysis

Applying traditional compartmental modelling, two configurations could describe the observed kinetics: a two-tissue, three rate constants sequential compartment model (A) or a two-tissue, three rate constants parallel compartment model (B). The sequential model (A) has been previously used to describe the irreversible binding of ligands such as ^{11}C-*N*-methylspiperone [30,31]. There, the irreversible uptake of the ligand as specified by the rate constant k_3 was the parameter which characterised the binding to the dopamine D_2 receptor sites. In other words, the specific binding of the radioligand to the receptor sites was represented by the irreversible accumulation of the radioactivity in tissue.

This means that the PET time-activity curve in a receptor-rich region differed from the time-activity curve in a region with lower receptor density by the slope of the irreversible binding component. Visual inspection of the time-activity curves reveals that within one subject there is no such slope difference between the regions. In fact the decay-corrected tissue time-activity curves of the different regions for one subject are almost parallel after 40 min. On the other hand, different slopes of the time-activity curves are observed between the four subjects. Therefore, the parallel compartmental model (B) was proposed to describe the kinetics of ^{11}C-SCH442416 in brain tissue. The parameter K_7 in this model is not related to specific binding of the radioligand to the receptor sites but is used to characterise nonspecific uptake.

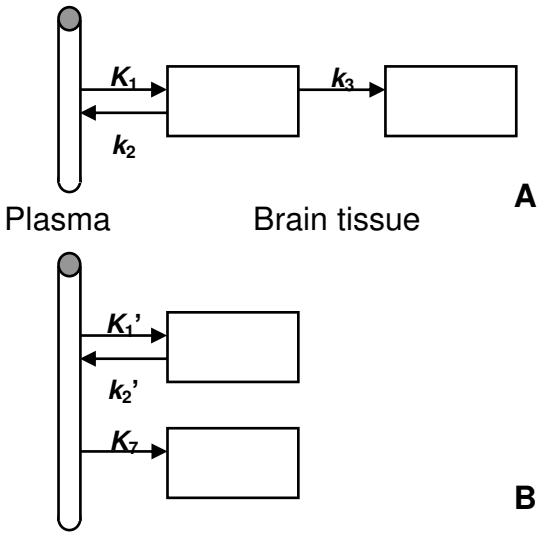

Figure 5. Two different layouts for the two-tissue compartment model for the description of irreversible uptake: (A) a sequential structure and (B) a parallel structure. These two structures are mathematically indistinguishable; they only differ in the interpretation of the model microparameters.

Spectral analysis [27] was used as a method to separate the various components of the tissue response curves representing irreversible binding, reversible binding, and a fast blood volume component. Regional parameter estimates for all four subjects are presented. The height of the irreversible spectral analysis peak in one subject is fairly constant across studied brain regions; however, there are considerable differences between the four scanned subjects in their irreversible uptake. The volumes of distribution V_T of the reversible peaks are lowest in the cerebellum which is devoid of A_{2A} receptors in humans, intermediate in the thalamus and highest in the regions comprising the striatum. This rank order is consistent with the known A_{2A} receptor distribution in the human brain [2].

Therefore, the V_T of the reversible binding of ^{11}C-SCH442416 appears to be correlated with the binding to the A_{2A} receptor sites. Assuming that the V_T describes free, non-specifically and specifically bound ligand in the brain tissue, estimates of regional binding potential BP_{ND} were calculated indirectly from the ratio of the target region over the cerebellar minus one and are listed in the last column. Mean binding potentials averaged across the left and right ROIs of the four subjects were calculated as 2.47 (putamen), 1.59 (caudate) and 0.53 (thalamus).

Furthermore, spectral analysis was also applied on the pixel level. In histograms of the volume of distribution are shown for two regions, the cerebellum and the striatum (combination of the putamen and caudate regions). The single peak in the fastest histogram bin on the right hand side at $\beta_{max} = 1\ s^{-1}$ ($\log_{10} \beta_{max} = 0$) represents the fractional blood volume.

	Height of the irreversible peak in s^{-1}	**Fractional blood volume (unitless)**	**Total volume of distribution V_T of the reversible peaks in (mL plasma) · (mL extravascular tissue)$^{-1}$**	**Calculated BP_{ND} (unitless)**
Subject 1				
Left Putamen	0.000231	0.019	0.25	2.85
Right Putamen	0.000254	0.026	0.26	2.94
Left Caudate	0.000234	0.019	0.18	1.72
Right Caudate	0.000215	0.021	0.15	1.33
Left Thalamus	0.000233	0.028	0.08	0.26
Right Thalamus	0.000235	0.027	0.09	0.32
Cerebellum	0.000199	0.026	0.07	
mean	**0.000229**			
Subject 2				
Left Putamen	0.000347	0.015	0.39	2.52
Right Putamen	0.000206	0.028	0.54	3.82
Left Caudate	0.000283	0.025	0.36	2.21
Right Caudate	0.000191	0.030	0.44	2.95
Left Thalamus	0.000260	0.033	0.21	0.91
Right Thalamus	0.000198	0.026	0.29	1.57
Cerebellum	0.000316	0.031	0.11	
mean	**0.000257**			
Subject 3				
Left Putamen	0.000160	0.022	0.33	2.53
Right Putamen	0.000180	0.025	0.32	2.39
Left Caudate	0.000174	0.023	0.21	1.21
Right Caudate	0.000162	0.030	0.23	1.45
Left Thalamus	0.000167	0.032	0.12	0.23
Right Thalamus	0.000154	0.029	0.12	0.27
Cerebellum	0.000149	0.031	0.09	
mean	**0.000164**			
Subject 4				
Left Putamen	0.000536	0.029	0.32	1.12
Right Putamen	0.000387	0.019	0.38	1.54
Left Caudate	0.000377	0.026	0.30	0.98
Right Caudate	0.000363	0.023	0.28	0.86
Left Thalamus	0.000347	0.033	0.22	0.44
Right Thalamus	0.000385	0.028	0.19	0.24
Cerebellum	0.000369	0.039	0.15	
mean	**0.000395**			

Table 1. Results from regional spectral analysis.

ISSN: 2057-3782 (Online)
http://dx.doi.org/10.17229/jdit.2014-0620-001

The difference between the histograms of the receptor-rich striatum and that of the cerebellum outlines the contribution of the specific binding to the total volume of distribution. Note that the irreversible peak in the leftmost bin at β_{min} = 5.663·x 10^{-4} s^{-1} ($\log_{10}$ β_{min} = -3.247) cannot been displayed as it corresponds to an infinite volume of distribution.

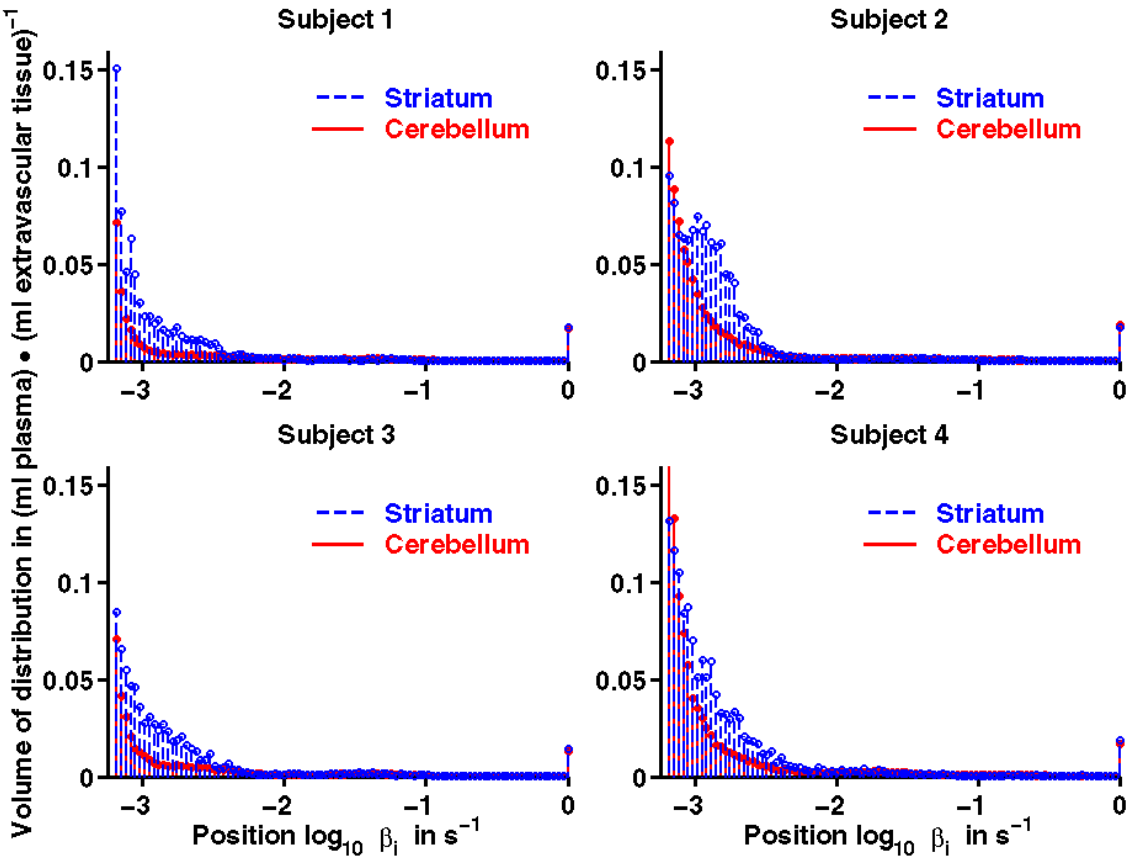

Figure 6. Histograms of the volume of distribution generated with spectral analysis on the pixel level for the cerebellum and the striatum (combination of the putamen and the caudate regions). The time constant of the radioactive decay of ^{11}C is 5.663·x 10^{-4} s^{-1} corresponding with the left end of the spectrum $\log_{10}$ β_{min} = -3.247.

3.4. Discussion

In this first-in-man study, the novel nonxanthine radioligand ^{11}C-SCH442416 for the measurement of A_{2A} receptor binding revealed two properties that set it aside from the majority of receptor ligands commonly used in molecular imaging.

First, the *in vivo* metabolism of ^{11}C-SCH442416 was found to be faster in humans than previously reported in rats [11] and in *macaca nemestrina* [13]. This had not been expected when the blood sampling and metabolite analysis protocol was originally devised therefore making a later adjustment of the scanning protocol necessary. This finding is also in contrast to what is observed with most PET radiotracers which are usually metabolised more rapidly in rodents than in man.

Second, most radioligands which are used in PET for the quantification of receptor availability bind reversibly within the time course of a PET scan which is typically two hours or less for a ^{11}C labelled compound. There are also examples of PET neuroreceptor studies with tracers which effectively bind irreversibly during the PET scan, ^{11}C-*N*-methylspiperone [30,31] being a prominent example. However, it is unusual for an irreversibly binding component to represent non-specific uptake which does not vary between brain regions with high and low concentration of binding sites.

From our data it is not clear what this slow, region independent and subject specific irreversible brain uptake reflects. The possibility that a brain penetrating, slowly accumulating and nonspecifically binding radiometabolite of ^{11}C-SCH442416 exists cannot be excluded unless brain tissue samples are investigated for their radiolabelled entities. However, the absence of radiolabelled compounds in the human plasma samples that are lipophilic and therefore would be considered to be likely to cross the blood-brain barrier by passive diffusion did not provide any support for the hypothesis that the slow and apparently irreversible tissue uptake is caused by the brain accumulation of a radiolabelled metabolite of ^{11}C-SCH442416. As the radiochemical purity of ^{11}C-SCH442416 prior to injection was always measured to exceed 99%, there is also no suggestion that co-injected radiolabelled impurities were responsible for the observed accumulation of nonspecifically binding radiolabel in the human brain.

Despite this difficulty, we have used the standard approach of quantification for reversibly binding radioligands [28] to obtain estimates of the *in vivo* binding potential of the nondisplaceable uptake BP_{ND}. The contribution of the irreversibly binding nonspecific uptake, as shown in the second column and expressed by the plasma-to-brain rate constant K_7 in the parallel compartmental model in B, does not enter into the indirect calculation of the binding potential BP_{ND}. Because the volume of distribution of a tissue compartment with a trap would be infinite [32], it was not possible to simply add the contribution of this irreversibly binding component of the nonspecific binding to the volume of distribution of the reversible nonspecific binding V_{NS} in the mathematical framework provided by Innis et al. [28]. Therefore the volume of distribution of the nonspecific binding V_{NS} that enters into the equation for the indirect calculation of the binding potential BP_{ND} only reflects the reversible nonspecific binding and not the irreversible nonspecific binding. As a consequence, the BP_{ND} obtained (see last column) are relatively large considering the modest additional binding of ^{11}C-SCH442416 in the A_{2A} rich target regions in comparison with the cerebellar reference region.

However, if ^{11}C-SCH442416 is for example to be used to estimate the A_{2A} receptor occupancy by a drug with affinity to these receptors in a dual PET scan paradigm (one tracer alone baseline scan and one blocked scan after drug administration), then the BP_{ND} as calculated here can still be used for the calculation of the per cent occupancy with the equation

$$Occ = \left(1 - \frac{BP_{ND}^{blocked}}{BP_{ND}^{baseline}}\right) \cdot 100\%$$

provided that the assumptions that are usually made in those studies, such as unchanged nondisplaceable binding between the two conditions [33], are met.

In this report, spectral analysis [27] was used to analyse the kinetics of ^{11}C-SCH442416 brain uptake at a regional and also a voxel level. This had the advantage over choosing a compartmental model that no *a priori* assumptions on the number of tissue compartments needed to appropriately describe the kinetics or on the reversibility of the binding had to be made. From the results obtained with spectral analysis, two compartmental models could be used to equally fit the data. These two model structures are mathematically indistinguishable, i.e. a given data set will be fitted by the model equations with the same residual sum of squared errors. The following correspondences allow the conversion of the microparameters between the two models:

$$K_1^{'} = \frac{K_1 \cdot k_2}{k_2 + k_3}$$

$$k_2^{'} = k_2 + k_3$$

$$K_7 = \frac{K_1 \cdot k_3}{k_2 + k_3}$$

However, only the model structure of B provides estimates of the total volume of distribution

$$V_T = \frac{K_1^{'}}{k_2^{'}}$$

that are equivalent to those obtained with spectral analysis reported in the penultimate column. The second parallel tissue compartment accounts for the irreversible nonspecific uptake of ^{11}C-SCH442416 with a single rate constant K_7 that is equivalent to the height of the irreversible peak in spectral analysis reported in the second column.

PET scans in more than four subjects studied here, and more than one scan per subject are needed to better characterise the pronounced intersubject variability in the binding of ^{11}C-SCH442416, and to characterize also the radioligand intrasubject variability. Furthermore, it is crucial to perform PET scans with ^{11}C-SCH442416 with subtype selective A_{2A} receptor blockers to provide proof of the specific and nonspecific binding components presented here. One study using a non-xanthine, selective A_{2A} receptor antagonist in development, vipadenant (previously known as BIIB014) has been reported [34], and the study using preladenant (product in development with the similar mechanism of action) will be reported in the future.

4. Conclusions

The pilot PET studies with ^{11}C-SCH442416 demonstrated the quantifiability of A_{2A} receptor binding in striatal regions of the human brain. Despite the fast kinetics and the small contribution of specific binding to the total tissue activity, specific binding parameters can be estimated with spectral analysis. Further studies using other available selective A_{2A} receptor blockers, will be important to fully validate the assumption on which the calculation of the binding potential is based on.

Conflicts of Interest

ID Grachev: Full-time employee of Schering-Plough Research Institute at the time of the study conduct and does not hold any stocks or shares, or have other financial competing interests.

DJ Brooks: Part-time employee of GE Healthcare at the time of the study conduct.

Acknowledgements

We gratefully acknowledge the staff of the Hammersmith PET Center, London, UK for successfully completing the PET scans; Imaging Research Solutions, Ltd (IRSL), Hammersmith Hospital, London, UK for the determination of specific binding potentials in the ROI, and the onsite manufacturing of ^{11}C-SCH 442416; Hammersmith Medicines Research, Central Middlesex Hospital, London, UK for successful management of subjects enrollment, performing all required study procedures and safety monitoring. We particularly thank Andy Blythe, Hope McDevitt, Stella Ahier, Andreanna Williams, Leonhard Schnorr and Abel Haida who made the acquisition of these scans possible, and Safiye Osman and Dr. Vincent J. Cunningham who helped with the data acquisition and analyses. Drs Adam McMahon, David Cutler, John Hunter and Steve Warrington receive our thanks for helpful discussions on the manuscript. This study was supported by Schering-Plough Research Institute, Kenilworth, NJ, USA. The radiotracer quantification data were presented at AMI/SNIDD International Conference, September 24-26, 2003, Madrid, Spain.

References

Key Article References: 1, 2, 13, 25 & 34

[1] Svenningsson P, Hall H, Sedvall G, Fredholm BB. Distribution of adenosine receptors in the postmortem human brain: an extended autoradiographic study. *Synapse*. 1997; 27: 322-335. [CrossRef] [PubMed Abstract]

[2] Svenningsson P, Le Moine C, Fisone G, Fredholm BB. Distribution, biochemistry and function of striatal adenosine A_{2A} receptors. *Prog Neurobiol*. 1999; 59: 355-396. [CrossRef] [PubMed Abstract]

[3] Stone-Elander S, Thorell JO, Eriksson L, Fredholm BB, Ingvar M. In vivo biodistribution of [*N*-^{11}C-methyl]KF 17837 using 3-D-PET: Evaluation as a ligand for the study of adenosine A_{2A} receptors. *Nucl Med Biol*. 1997; 24: 187-191. [PubMed Abstract]

[4] Noguchi J, Ishiwata K, Wakabayashi S, et al. Evaluation of carbon-11-labeled KF17837: a potential CNS adenosine A_{2a} receptor ligand. *J Nucl Med*. 1998; 39: 498-503. [PubMed Abstract] [Reference Source]

[5] Ishiwata K, Noguchi J, Wakabayashi S, et al.^{11}C-labeled KF18446: A potential central nervous system adenosine A_{2a} receptor ligand. *J Nucl Med*. 2000; 41: 345-354. [PubMed Abstract] [Reference Source]

[6] Hirani E, Gillies J, Karasawa A, et al. Evaluation of [4-*O-methyl*-^{11}C]KW-6002 as a potential PET ligand for mapping central adenosine A_{2A} receptors in rats. *Synapse*. 2001; 42: 164-176. [CrossRef] [PubMed Abstract]

[7] Brooks DJ, Doder M, Osman S, et al. Positron emission tomography analysis of [^{11}C]KW-6002 binding to human and rat adenosine A_{2A} receptors in the brain. *Synapse*. 2008; 62: 671-681. [PubMed Abstract]

[8] Ishiwata K, Mishina M, Kimura Y, Oda K, Sasaki T, Ishii K. First visualization of adenosine A_{2A} receptors in the human brain by positron emission tomography with [^{11}C]TMSX. *Synapse* 2005; 55: 133-136. [CrossRef] [PubMed Abstract]

[9] Naganawa M, Kimura Y, Mishina M, et al. Quantification of adenosine A_{2A} receptors in the human brain using [^{11}C]TMSX and positron emission tomography. *Eur J Nucl Med Mol Imaging*. 2007; 34: 679-687. [CrossRef] [PubMed Abstract]

[10] Mishina M, Ishiwata K, Kimura Y, et al. Evaluation of distribution of adenosine A_{2A} receptors in normal human brain measured with [^{11}C]TMSX PET. *Synapse*. 2007; 61: 778-784. [CrossRef] [PubMed Abstract]

[11] Todde S, Moresco RM, Simonelli P, et al. Design, radiosynthesis, and biodistribution of a new potent and selective ligand for in vivo imaging of the adenosine A_{2A} receptor system using positron emission tomography. *J Med Chem*. 2000; 43: 4359-4362. [PubMed Abstract]

[12] Hinz R, Grachev ID, Cutler DL, et al. In-vivo quantification of A_{2A} receptors in human brain with [^{11}C]SCH442416 and positron emission tomography. *Mol Imaging Biol*. 2003; 5: 1656-1665. [PubMed Abstract] [PMC Free Article]

[13] Moresco RM, Todde S, Belloli S, et al. In vivo imaging of adenosine A_{2A} receptors in rat and primate brain using [^{11}C]SCH442416. *Eur J Nucl Med Mol Imaging*. 2005; 32: 405-413. [CrossRef] [PubMed Abstract]

[14] Mihara T, Noda A, Arai H, et al. Brain adenosine A_{2A} receptor occupancy by a novel A_1/A_{2A} receptor antagonist, ASP5854, in rhesus monkeys: relationship to anticataleptic effect. *J Nucl Med*. 2008; 49:1183-1188. [CrossRef] [PubMed Abstract]

[15] Spinks TJ, Jones T, Bloomfield PM, et al. Physical characteristics of the ECAT EXACT3D positron tomograph. *Phys Med Biol*. 2000; 45: 2601-2618. [CrossRef] [PubMed Abstract]

[16] Spinks TJ, Miller MP, Bailey DL, Bloomfield PM, Livieratos L, Jones T. The effect of activity outside the direct field of view in a 3D-only whole-body positron tomograph. *Phys Med Biol.* 1998; 43: 895-904. [CrossRef] [PubMed Abstract]

[17] Watson CC, Newport DF, Casey ME. A single scatter simulation technique for scatter correction in three-dimensional PET. In: Grangeat P, Amans J-L, eds. *Three-Dimensional Image Reconstruction in Radiology and Nuclear Medicine*. Dordrecht: Kluwer; 1996: 255-268. [CrossRef]

[18] Ranicar AS, Williams CW, Schnorr L, et al. The on-line monitoring of continuously withdrawn arterial blood during PET studies using a single BGO/photomultiplier assembly and non-stick tubing. *Med Prog Technol.* 1991; 17: 259-264. [PubMed Abstract]

[19] Luthra SK, Osman S, Turton DR, Vaja V, Dowsett K, Brady F. An automated system based on solid phase extraction and HPLC for the routine determination in plasma of unchanged [^{11}C]-L-deprenyl; [^{11}C]diprenorphine; [^{11}C]flumazenil; [^{11}C]raclopride; and [^{11}C]SCH23390. *J Lab Comp Radiopharm.* 1993; 32: 518-520.

[20] Studholme C, Hill DL, Hawkes DJ. Automated three-dimensional registration of magnetic resonance and positron emission tomography brain images by multiresolution optimization of voxel similarity measures. *Med Phys.* 1997; 24: 25-35. [CrossRef] [PubMed Abstract]

[21] Hammers A, Koepp MJ, Free SL, et al. Implementation and application of a brain template for multiple volumes of interest. *Hum Brain Mapp.* 2002; 15: 165-174. [PubMed Abstract]

[22] Hammers A, Allom R, Koepp MJ, et al. Three-dimensional maximum probability atlas of the human brain, with particular reference to the temporal lobe. *Hum Brain Mapp.* 2003; 19: 224-247. [CrossRef] [PubMed Abstract]

[23] Robb RA, Barillot C. Interactive display and analysis of 3-D medical images. *IEEE Trans Med Imag.* 1989; 8: 217-226. [CrossRef] [PubMed Abstract]

[24] Robb RA, Hanson DP, Karwoski RA, Larson AG, Workman EL, Stacy MC. ANALYZE: a comprehensive, operator-interactive software package for multidimensional medical image display and analysis. *Computerized Medical Imaging and Graphics* 1989; 13: 433-454. [CrossRef] [PubMed Abstract]

[25] Hinz R, Turkheimer FE. Determination of tracer arrival delay with spectral analysis. *IEEE Trans Nucl Sci* 2006; 53: 212-219. [CrossRef]

[26] Gunn RN, Sargent PA, Bench CJ, et al. Tracer kinetic modeling of the 5-HT$_{1A}$ receptor ligand [*carbonyl*-^{11}C]WAY- 100635 for PET. *Neuroimage*. 1998; 8: 426-440. [PubMed Abstract]

[27] Cunningham VJ, Jones T. Spectral analysis of dynamic PET studies. *J Cereb Blood Flow Metab.* 1993; 13: 15-23. [CrossRef] [PubMed Abstract]

[28] Innis RB, Cunningham VJ, Delforge J, et al. Consensus nomenclature for in vivo imaging of reversibly binding radioligands. *J Cereb Blood Flow Metab*. 2007; 27: 1533-1539. [CrossRef] [PubMed Abstract]

[29] Lawson, CL, Hanson, RJ. *Solving least squares problems*. Philadelphia, PA: Society for Industrial and Applied Mathematics; 1995. [CrossRef]

[30] Wong DF, Gjedde A, Wagner HN Jr. Quantification of neuroreceptors in the living human brain. I. Irreversible binding of ligands. *J Cereb Blood Flow Metab.* 1986; 6: 137-146. [CrossRef] [PubMed Abstract]

[31] Wong DF, Gjedde A, Wagner HNJr, et al. Quantification of neuroreceptors in the living human brain. II. Inhibition studies of receptor density and affinity. *J Cereb Blood Flow Metab*. 1986; 6: 147-153. [CrossRef] [PubMed Abstract]

[32] Gunn RN, Gunn SR, Cunningham VJ. Positron emission tomography compartmental models. *J Cereb Blood Flow Metab*. 2001; 21: 635-652. [CrossRef] [PubMed Abstract]

[33] Hinz R, Selvaraj S, Murthy VN et al. Effects of citalopram infusion on the serotonin transporter binding of [^{11}C]DASB in healthy controls. *J Cereb Blood Flow Metab*. 2008; 28: 1478-1490. [CrossRef] [PubMed Abstract]

[34] Brooks DJ, Papapetropoulos S, Vandenhende F et al. An open-label, positron emission tomography study to assess adenosine A2A brain receptor occupancy of vipadenant (BIIB014) at steady-state levels in healthy male volunteers. *Clin Neuropharmacol*. 2010; 33(2):55-60. [CrossRef] [PubMed Abstract]

Citation: Grachev ID, Doder M, Brooks DJ, Hinz R. Quantitative *in vivo* Imaging of Adenosine A_{2A} Receptors in the Human Brain Using ^{11}C-SCH442416 PET: A Pilot Study. *Journal of Diagnostic Imaging in Therapy*. 2014; 1(1): 1-19.
http://dx.doi.org/10.17229/jdit.2014-0620-001

Received: 3 June 2014 | **Revised:** 20 June 2014 | **Accepted:** 20 June 2014

Published Online 20 June 2014 (http://www.openmedscience.com)